applied sciences

MDPI

Article

Predictable Trajectory Planning of Industrial Robots with Constraints

Youdong Chen * and Ling Li

School of Mechanical Engineering and Automation, Beihang University, Beijing 100191, China; liuyunmuzi@126.com

* Correspondence: chenyd@buaa.edu.cn; Tel.: +86-1369-312-7687

Received: 6 November 2018; Accepted: 7 December 2018; Published: 17 December 2018

Abstract: Trajectory prediction is currently attracting considerable attention. This paper proposes geodesic trajectory planning with end-effector and joint constraints to predict the trajectory properties of the end-effector, such as velocities, accelerations, and smoothness. The prediction of the trajectory properties is independent of the joint trajectories. The prediction makes it possible to adjust the trajectory properties in line with a light computational burden. To demonstrate the effectiveness of the proposed method, experiments were conducted using the Efort robot. The experiments show that the proposed method can predict the properties of the trajectory and modify the trajectory to meet the constraints.

Keywords: predictable trajectory planning; geodesic; constrained motion

1. Introduction

There are growing interests in trajectory prediction. Trajectory prediction can be classified into two kinds: trajectory prediction for future time and trajectory prediction for future tasks. Future actions have been predicted for obstacle avoiding and trajectory re-planning [1,2]. Appropriate trajectories for future tasks have been predicted by using machine learning [3,4]. Fast motion planning has been obtained from experience. The transfer of previously optimized trajectories to a new situation cannot be made in the joint space. Little attention has been paid to Cartesian trajectory prediction that predicts the motion performed by the robot end-effector under joint velocity/acceleration constraints.

Many practical tasks impose constraints on robot motions, such as machining, welding, and cutting and so on. RRT (rapidly-exploring random tree)/PRM (probabilistic roadmap)-based approaches were used to plan the path with end-effector constraints [5–9]. The Cartesian positions of the end-effector at the via-points were achieved, but the motions of the end-effector between via points are not predictable, in view of the nonlinear effects introduced by the direct kinematics.

There are limits of joint positions, velocities, and accelerations. To obtain smooth motions, the joint constraints should be bounded. Joint constraints are often met by optimizing appropriate objective functions, such as keeping the joints close to their range centers [10], using the joint ranges in a weighted pseudo-inversion [11], or defining an infinity norm to be minimized at the velocity levels [12]. However, this method did not track the assigned paths. Inverse kinematics was used to enable joint velocity and acceleration not exceeding their limits [13], which was achieved by scaling the task time. However, these methods cannot meet joint constraints.

Generally, there are three questions. (1) The motions of the end-effector between via points are not predictable in trajectory planning with end-effector constraints. (2) There is no guarantee that the end-effector will track the assigned paths in trajectory planning with joint constraints. (3) End-effector constraints and joint constraints have seldom been considered simultaneously in the previous studies. In this paper, we attempt to solve these problems.

Geodesic is an important concept in Riemannian geometry and can be used in robot trajectory planning [14,15] and machine tool interpolation [16]. By selecting suitable Riemannian metrics and local coordinates, the direct output of the proposed method is joint trajectories.

In this paper, we present a predictable trajectory planning with constraints using geodesics. The end-effector position, velocities, and accelerations can be predicted without forward kinematics. The prediction of end-effector motion properties can be obtained before the calculation of the geodesic method. While tracking the constrained end-effector paths, the joint velocity/acceleration constraints can be met by scaling the motion time. The trajectory based on this method is predictable and has a light computational burden. Furthermore, the end-effector motions are of high precision.

This paper is organized as follows. The predictable trajectory planning with constraints is presented in Section 2. Using null constraints and a virtual end-effector constraint, predictable linear and circular trajectory planning are described in Section 3. Experiments using the Efort robot are illustrated in Section 4. Finally, the conclusion is given.

2. Predictable Trajectory Planning with Constraints

2.1. Predictable Trajectory Planning with End-Effector Constraints

The robot end-effector moves under some constraints to accomplish some tasks in practical applications. The end-effector position constraint H and orientation constraint F can be described by

$$\begin{cases} H(p) = 0 \\ F(n, o, a) = 0 \end{cases} \tag{1}$$

where p and $\begin{Bmatrix} n & o & a \end{Bmatrix}$ are the end-effector position and orientation respectively.

The end-effector trajectories in Cartesian space can be predicted without forward kinematics. The prediction is independent of the joint trajectories and can be made before the calculation of the proposed geodesic method. The prediction can adjust the end-effector motion properties and has light computational burdens.

First of all, the corresponding Cartesian paths meet the end-effector constraints defined in Equation (1). In Cartesian space, the end-effector moves the shortest paths that are usually not linear paths. Because the linear paths may not satisfy the end-effector constraints the shapes of the Cartesian paths are determined by the constraints.

Secondly, the Cartesian velocity is constant. Because the velocity of a geodesic is constant, the velocity always equal to the initial velocity. The velocity of a geodesic trajectory v is

$$v = \frac{L_d}{t_w} = v_0, \tag{2}$$

where L_d, t_w and v_0 are the path length, the motion time, and the initial velocity, respectively.

Because the velocity of a geodesic is constant, the end-effector performs a uniform curved motion. The tangential acceleration is zero. The centripetal acceleration a is

$$a = \frac{v^2}{r}, \tag{3}$$

where r is the radius of the curvature of a geodesic path.

Finally, the joint and Cartesian trajectories are both smooth. Because the solutions of the geodesic equations are C^3 continuous [10], the joint trajectories are smooth as are the Cartesian trajectories.

The joint trajectories are calculated by the geodesic method. The position and orientation are the functions of the joint variables,

$$\begin{aligned} p &= p(q_1 \cdots q_k) \\ n &= n(q_{k+1} \cdots q_n) \\ o &= o(q_{k+1} \cdots q_n) \\ a &= a(q_{k+1} \cdots q_n) \end{aligned} \tag{4}$$

where q_i are joint variables. By the implicit function theorem [17], there are q_{i_0} and q_{j_0} which are derived from Equation (1)

$$\begin{aligned} q_{i_0} &= q_{i_0}(q_1, \cdots q_{i_0-1}, q_{i_0+1}, \cdots q_{k_0}) \\ q_{j_0} &= q_{j_0}(q_{k_0+1}, \cdots q_{j_0-1}, q_{j_0+1}, \cdots q_n) \end{aligned} \tag{5}$$

The position and orientation vectors can be described as,

$$\begin{aligned} p &= p(q_1, \cdots q_{i_0-1}, q_{i_0+1}, \cdots q_{k_0}) \\ \mathrm{O} \cong n + o + a &= \mathrm{O}(q_{k_0+1}, \cdots q_{j_0-1}, q_{j_0+1}, \cdots q_n) \end{aligned} \tag{6}$$

In this way, the end-effector constraints are implicit in the position and orientation vector. For simplicity, they can be denoted as,

$$\begin{aligned} u_i &= \begin{cases} q_i, i \le i_0 - 1 \\ q_{i+1}, k_0 \ge i \ge i_0 + 1 \end{cases} \\ v_i &= \begin{cases} q_{k+i}, i \le j_0 - k_0 - 1 \\ q_{k+i+1}, n \ge i \ge j_0 + 1 \end{cases} \\ p &= (p_1, p_2, p_3) \\ \mathrm{O} &= (\mathrm{O}_1, \mathrm{O}_2, \mathrm{O}_3) \end{aligned} \tag{7}$$

Define Riemannian metrics as

$$\begin{aligned} {}^d g &= \sum_{\alpha,i,j} \frac{\partial p_\alpha}{\partial u_i} \frac{\partial p_\alpha}{\partial u_j} du_i du_j = \sum_{i,j} {}^d g_{ij} du_i du_j \\ {}^o g &= \sum_{\alpha,i,j} \frac{\partial \mathrm{O}_\alpha}{\partial v_i} \frac{\partial \mathrm{O}_\alpha}{\partial v_j} dv_i dv_j = \sum_{i,j} {}^o g_{ij} dv_i dv_j \end{aligned} \tag{8}$$

where du_i is the differential of u_i, and $\Sigma_{\alpha,i,j}$ is the summation notation with the index α, i, j. The quantities relevant position and orientation with superscript are d and o, respectively. The geodesic equations are

$$\begin{cases} \frac{d^2 u_i}{dt^2} + \sum_{k,j} {}^d\Gamma^i_{kj} \frac{du_k}{dt} \frac{du_j}{dt} = 0 \\ \frac{d^2 v_l}{dt^2} + \sum_{m,b} {}^o\Gamma^l_{bm} \frac{dv_m}{dt} \frac{dv_b}{dt} = 0 \end{cases} \tag{9}$$

The Christoffel symbols ${}^d\Gamma^i_{kj}$ and ${}^o\Gamma^l_{mb}$ are given as

$$\begin{cases} {}^d\Gamma^i_{kj} = \frac{1}{2} \sum_m {}^d g^{ei} \left(\frac{\partial^d g_{ke}}{\partial u_j} + \frac{\partial^d g_{je}}{\partial u_k} - \frac{\partial^d g_{kj}}{\partial u_e} \right) \\ {}^o\Gamma^l_{bm} = \frac{1}{2} \sum_f {}^o g^{fl} \left(\frac{\partial^o g_{nf}}{\partial v_m} + \frac{\partial^o g_{mf}}{\partial v_b} - \frac{\partial^o g_{bm}}{\partial v_f} \right) \end{cases} \tag{10}$$

where ${}^d g^{ei}$ and ${}^o g^{fl}$ are the elements of inverse Riemannian metric coefficient matrices ${}^d G^{-1} = \left({}^d g_{ij} \right)^{-1}$ and ${}^o G^{-1} = \left({}^o g_{mn} \right)^{-1}$ respectively [16]. ∂ is the notation of partial differential. The Christoffel

symbols are derived from the position and orientation vectors with end-effector constraints. The joint trajectories are obtained by Equation (9) together with Equations (5) and (7) with boundary conditions

$$\begin{cases} u_i(t_0) = {}^0u_i \\ v_l(t_0) = {}^0v_l \\ u_i(t_0 + t_w) = {}^fu_i \\ v_l(t_0 + t_w) = {}^fv_l \end{cases} \tag{11}$$

where t_0, $\left\{{}^0u_i, {}^0v_l\right\}$ and $\left\{{}^fu_i, {}^fv_l\right\}$ are the start time, the start and end joint positions, respectively. In other words, the direct output of the geodesic method is joint trajectories.

As we can see above, trajectory planning with the end-effector constraints is given. The prediction of the end-effector motion properties can be made before the calculation of the geodesic method. The prediction is demonstrated in Section 3.1 in a simple way. The reason why the trajectories can be predicted is that they are geodesic trajectories. Geodesic has many merits, such as the shortest path, constant velocity.

2.2. Joint Velocity/Acceleration Limits Avoidance

The joint velocity and acceleration limits must be taken into account. Assume that the trajectory planned by the proposed method is,

$$\left\{t_w, q_i, \dot{q}_i, \ddot{q}_i (i = 1, \cdots, n)\right\} \tag{12}$$

Introducing a set of joint velocity/acceleration limits as follows,

$$\begin{cases} \left|\dot{q}_i\right| \leq \dot{q}_{i,\text{lim}} \\ \left|\ddot{q}_i\right| \leq \ddot{q}_{i,\text{lim}} \end{cases} \tag{13}$$

where $\dot{q}_{i,\text{lim}}$ and $\ddot{q}_{i,\text{lim}}$ are the velocity and acceleration limits of the ith joint. Define a scaling factor

$$\alpha = \max\left\{\frac{\left|\dot{q}_i\right|}{\dot{q}_{i,\text{lim}}}, \frac{\left|\ddot{q}_i\right|}{\ddot{q}_{i,\text{lim}}}, i = 1, \cdots, n\right\} \tag{14}$$

If $\alpha \geq 1$, there is at least one of the joint velocities or accelerations out of its limit. Update the motion time by the scaling factor,

$$t_{new} = \alpha t_w \tag{15}$$

The end-effector motions are predictable. The end-effector moves along the desired paths. The end-effector velocity is renewed as,

$$v_{new} = \frac{1}{\alpha} v \tag{16}$$

Along the geodesic path, the tangential acceleration is still zero. The centripetal acceleration is

$$a_{new} = \frac{{v_{new}}^2}{r} = \frac{1}{\alpha^2} a \tag{17}$$

The new joint trajectories are obtained by solving the geodesic equations, Equation (9) under the updated motion time with the boundary conditions,

$$\begin{cases} u_i(t_0) = {}^0u_i \\ v_l(t_0) = {}^0v_l \\ u_i(t_0 + t_{new}) = {}^fu_i \\ v_l(t_0 + t_{new}) = {}^fv_l \end{cases} \tag{18}$$

Actually, the joint velocity and acceleration limits avoidance is achieved by scaling the motion time. Our method can track the assigned paths, and the velocities while the accelerations can be predicted in advance.

2.3. Acceleration/Deceleration Profile

Because the geodesic is constant-speed, the planning geodesic trajectory is constant speed. The acceleration/deceleration profile should be considered at the endpoints in the practical applications.

Generally, the acceleration/deceleration profile is given as

$$\frac{d^2q_i}{dt^2} + \sum_{k,j} \Gamma^i_{kj} \frac{dq_k}{dt} \frac{dq_j}{dt} = \frac{acc}{\sqrt{\sum_j (\frac{dq_j}{dt})^2}} \frac{dq_i}{dt} \tag{19}$$

where Γ^i_{kj} and acc are the Christoffel symbols and the acceleration respectively [10]. In fact, acc is the tangential acceleration. For linear motions, the centripetal acceleration equals zero. The tangential acceleration is the acceleration acc. The acceleration of curved motions acc is actually the tangential acceleration.

3. Predictable Linear and Circular Trajectory Planning

3.1. Predictable Linear Trajectory Planning

If the constraint defined in Equation (1) is zero, the method illustrated in Section 2 degenerates into linear trajectory planning. Because the shortest path in the Cartesian space is a linear path, the Riemannian metrics ${}^dg$ and ${}^og$ become [9],

$$\begin{cases} {}^dg = (dp)^2 \\ {}^og = (dn)^2 + (do)^2 + (da)^2 \end{cases} \tag{20}$$

The geodesic equations are

$$\begin{cases} \frac{d^2q_i}{dt^2} + \sum_{k,j} {}^d\Gamma^i_{kj} \frac{dq_k}{dt} \frac{dq_j}{dt} = 0 \\ \frac{d^2q_l}{dt^2} + \sum_{m,b} {}^o\Gamma^l_{bm} \frac{dq_b}{dt} \frac{dq_n}{dt} = 0 \end{cases} \tag{21}$$

We predict that the end-effector performs linear paths with the joint trajectories derived by Equation (19). The velocity and acceleration are constant and zero respectively. The Cartesian trajectories are smooth. These predictions are validated as follows.

The joint variables $\theta_1, \cdots, \theta_{k_0}$ are regarded as local coordinates of the position space. The components of the position vector p_x, p_y and p_z can also be chosen as coordinates. The Riemannian metric defined in Equation (19) can be rewritten as

$${}^dg = (dp)^2 = \begin{pmatrix} dp_x & dp_y & dp_z \end{pmatrix} I \begin{pmatrix} dp_x & dp_y & dp_z \end{pmatrix}^T, \tag{22}$$

where I is a 3×3 identity matrix. The geodesic equations become

$$\begin{cases} \frac{d^2 p_x}{dt^2} = 0 \\ \frac{d^2 p_y}{dt^2} = 0 \\ \frac{d^2 p_z}{dt^2} = 0 \end{cases} \tag{23}$$

which are equations of the linear path. Since geodesic has no relation to the coordinates, Equations (19) and (21) represent the same geodesic. The robot end-effector will move linearly under the joint trajectories determined by Equation (19). The velocity and acceleration are constant and zero respectively from Equation (21). The end-effector motion properties can be made before the calculation of the geodesic method. The Cartesian trajectories are smooth by the theory of the ordinary differential equation.

3.2. Predictable Circular Trajectory Planning

A geodesic of a spherical surface is a big circle. To obtain circular geodesic trajectory planning, we can impose a virtual end-effector constraint as

$$(p - p_0)^2 = R^2, (R > 0) \tag{24}$$

where p_0 and R are the center and the radius of a spherical surface respectively. The corresponding Riemannian metrics and geodesic equations can be obtained as in Section 2.

It is predicted that the end-effector performs circular paths with joint trajectories derived by the geodesic equations. The velocity, tangential acceleration, and centripetal acceleration are constant v, zero, and $\frac{v^2}{R}$ respectively. The Cartesian trajectories are smooth. Similar validation can be obtained.

4. Experiment

The proposed predictable trajectory planning method and joint velocity/acceleration limits avoidance schemes were validated in the following experiment. The experiment used a 6-DOF industrial robot Efort robot (ER3A-3C (HD)) produced by Anhui Efort intelligent equipment Co., Ltd. The link parameters of the Efort robot are shown in Table 1. The joint velocity limits given by the manufacture are presented in Table 2. The joint acceleration limit is 2×10^4 (rad/s^2).

Table 1. Link parameters of the Efort robot.

i	α_{i-1}	a_{i-1} (mm)	d_i(mm)	θ_i
1	0	0	0	θ_1
2	$-\pi/2$	50	0	θ_2
3	0	270	0	θ_3
4	$-\pi/2$	70	299	θ_4
5	$\pi/2$	0	0	θ_5
6	$-\pi/2$	0	0	θ_6

Table 2. The joint velocity limits of the Efort robot.

Joint	1	2	3	4	5	6
limits(rad/s)	4.01	4.01	4.36	5.59	5.59	7.33

An actual machining process is performed on the Efort robot. The coordinates and time stamps of the via points on the machined path are listed in Table 3. The paths are shown in Figure 1. The desired Cartesian velocity is 800 mm/s. To reduce the vibration, the Cartesian velocities at the corner points are set at 200 mm/s.

Before the experiment, we can predict the trajectories. The robot will move along the path shown in Figure 1 with the end-effector constraints. There will be an acceleration zone, a constant-velocity zone and a deceleration zone in a normal block. In a short block, there will be only an acceleration/deceleration zone or a constant-velocity zone. After avoiding the joint limits, the end-effector will move the desired path. The motion time and velocities will be scaled.

In the constant-velocity zones, the trajectories are generated by Equation (19). The trajectories in the acceleration and deceleration zones are generated by Equation (17). The corresponding results are shown in Figure 2. In the first acceleration zone, the velocity creeps up from 0 to 200 mm/s in 0.2 s. The velocity runs to 800 mm/s within 0.04 s. The total motion time grows from 6.18 s to 6.49 s with the joint avoidance scheme. Corresponding velocities are also changed.

The joint trajectories are shown in Figure 3. As shown in Table 4, the maximum velocity and the maximum acceleration of joint 3 are 5.06 rad/s and 2.32 $\times$ 104 rad/s2, respectively. Both of the values exceed their limits. The method of joint velocity/acceleration limits avoidance introduced in Section 2.2 is employed to adjust the joint velocity and acceleration trajectories. Actually, there are three areas where the joint velocities exceed their limits. These trajectories can be modified to comply with the velocity and acceleration constraints by scaling the motion time. Scaling the neighboring zones using the scaling factor defined in Equation (12), the motion time is updated by the scaling factor as in Equation (13). The maximum velocity and the maximum acceleration of joint 3 reduced to 4.36 rad/s and 1.85 $\times$ 104 rad/s2. The maximum joint velocities and accelerations are shown in Table 4. Table 4 shows that most of the values are reduced and all values are in the allowable range. The modified joint trajectories are shown in Figure 3. To see the details clearly, the first modified zone is taken as an example, as shown in Figure 4. In this zone, the motion time (0.48–0.76) (s) is scaled to (0.48–0.85) (s). The velocity of the constant-velocity zone is reduced from 800 mm/s to 592.57 mm/s, as shown in Figure 2. The Cartesian paths marked red in Figure 1 are the joint modified zones. The Cartesian path marked green in Figure 1 is above the plane. As is shown, the predicted Cartesian path coincides with the modified test one. The Cartesian velocity shown in Figure 2 is consistent with the predictions that are acceleration, constant velocity, and deceleration zones. It can be observed that the proposed method allows us to keep the joint velocities and accelerations below their limits while precisely tracking the desired paths. The machined workpiece is shown in Figure 5. The computational time of each interpolation point is about 1ms, which meets the real time demands. The Cartesian trajectories move as is predicted.

Table 3. The coordinates and time stamps of the via points.

	(px, py, pz) (mm)	Time (s)		(px, py, pz) (mm)	Time (s)
1	(500, −260, 100)	0	14	(310, −70, 80)	2.89
2	(500, −260, 80)	0.2	15	(310, −70, 100)	2.99
3	(500, −60, 80)	0.48	16	(355, −115, 100)	3.31
4	(300, −60, 80)	0.76	17	(355, −115, 80)	3.41
5	(300, −260, 80)	1.04	18	(355, −205, 80)	3.86
6	(500, −260, 80)	1.32	19	(310, −160, 80)	4.18
7	(500, −260, 100)	1.42	20	(310, −160, 100)	4.28
8	(490, −250, 80)	1.49	21	(445, −205, 100)	4.99
9	(490, −250, 100)	1.59	22	(445, −205, 80)	5.09
10	(490, −70, 80)	1.83	23	(400, −250, 80)	5.41
11	(310, −70, 80)	2.07	24	(355, −205, 80)	5.72
12	(490, −250, 80)	2.41	25	(490, −70, 80)	5.98
13	(310, −250, 80)	2.65	26	(490, −70, 100)	6.18

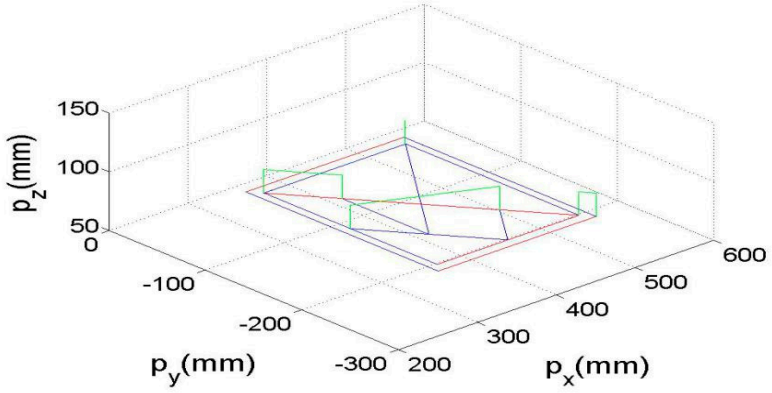

Figure 1. The Cartesian path of the Efort robot.

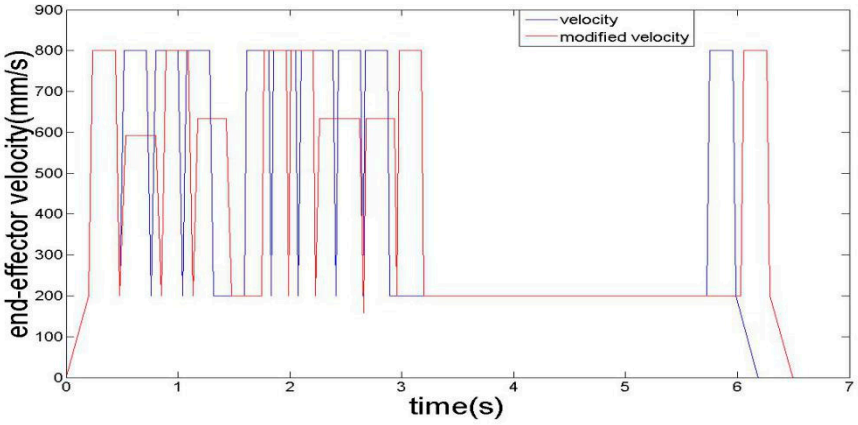

Figure 2. The Cartesian velocity of the Efort robot.

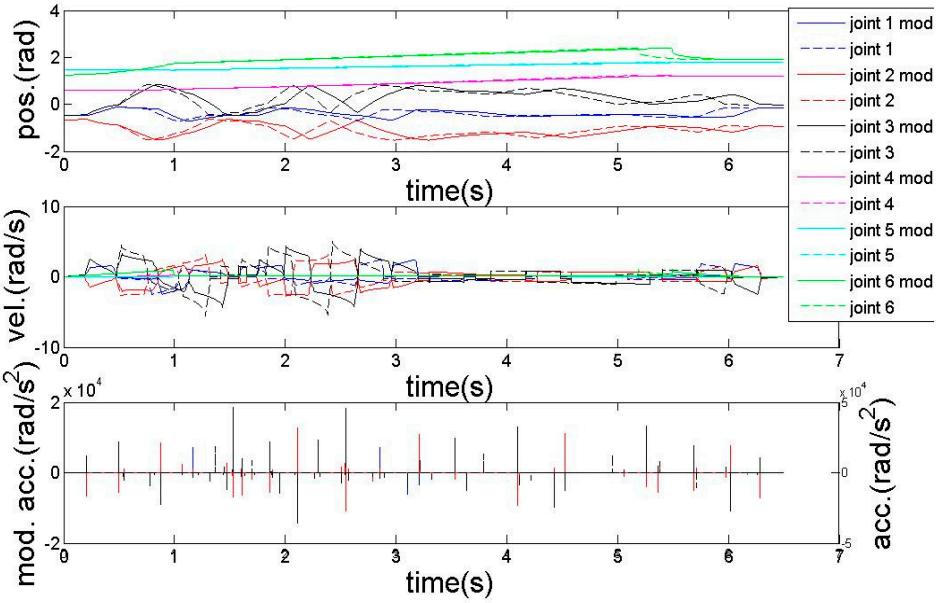

Figure 3. The joint trajectories (Here, pos., vel., acc., mod. are the abbreviation of position, velocity, acceleration and modified, respectively).

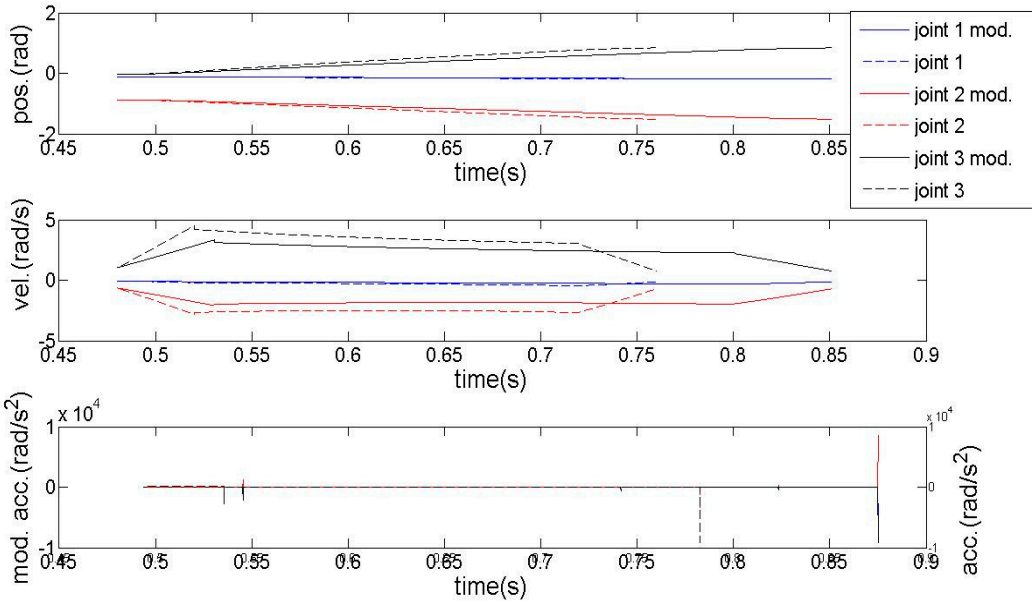

Figure 4. The local joint trajectories of first three joints (Here, pos., vel., acc., mod. are the abbreviation of position, velocity, acceleration and modified, respectively.).

Table 4. Comparisons of joint velocities and accelerations.

	Max. Vel. (rad/s)	Max. Modified Vel. (rad/s)	Max. Acc. (rad/s^2)	Max. Modified Acc. (rad/s^2)
joint 1	2.49	2.49	7.12 × 103	7.10 × 103
joint 2	3.21	2.73	1.37 × 104	1.28 × 104
joint 3	5.51	4.36	2.32 × 104	1.85 × 104
joint 4	0.22	0.22	450.47	214.25
joint 5	0.1	0.1	3.25 × 103	3.16 × 103
joint 6	0.1	0.1	1.67 × 104	1.61 × 104

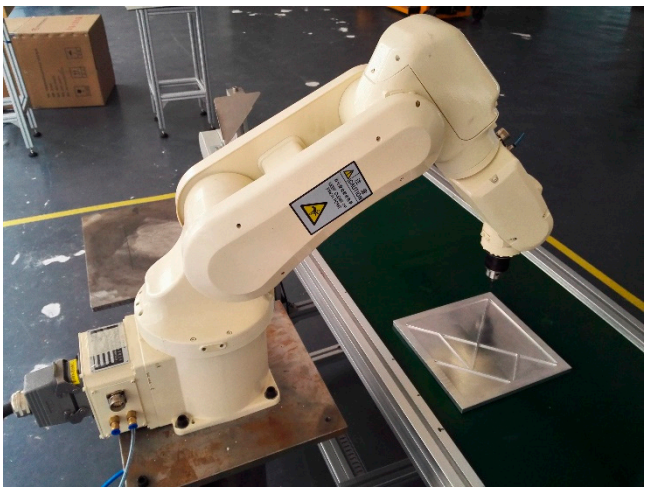

Figure 5. A machined workpiece.

5. Conclusions

In this paper, a predictable trajectory planning of industrial robots with constraints is presented. The end-effector and joint velocity/acceleration constraints are all considered. The end-effector motions, velocities, and accelerations can be predicted. The prediction is embedded in two aspects. (1) The direct output of the method is the joint trajectories while the Cartesian trajectories even between

via points can be predicted. (2) The end-effector paths can be predicted with velocity and acceleration constraints. Experiments with this method using the Efort robot are given. The results show that the trajectory can be predicted and modified on-line to meet the robot constraint.

There are also some limitations. In practice, the end-effector constraints may not be described easily. In the paper, we give two specific end-effector constraints—linear and circular end-effector motions. There are two ways to deal with complicated end-effector constraints. One is to explore the equations of end-effector constraints as in Equation (1). The other is to fit complex end-effector motions by linear and circular motions.

There are also questions to be studied, such as the accuracy of the prediction. Related problems include the size, influence factor, and improvements of the accuracy of the prediction, and so on.

Author Contributions: Y.C. and L.L. conceived and designed the experiments, L.L. performed the experiments, Y.C. and L.L. analyzed the data, L.L. contributed materials/analysis tools, L.L. wrote the original draft preparation, Y.C.; wrote the review and editing, Y.C. acquired the funding.

Funding: This research was funded by the Beijing Science and Technology Plan (D161100003116002).

Conflicts of Interest: The authors declare no conflict of interest.

References

1. Vendrell, E.; Mellado, M.; Crespo, A. Robot planning and re-planning using decomposition, abstraction, deduction, and prediction. *Eng. Appl. Artif. Intell.* **2001**, *14*, 505–518. [CrossRef]
2. Mora, M.C.; Tornero, J. Predictive and multirate densor-based planning under uncertainty. *IEEE Trans. Intell. Transp. Syst.* **2015**, *16*, 1493–1504. [CrossRef]
3. Jetchev, N.; Toussaint, M. Fast motion planning from experience: Trajectory prediction for speeding up movement generation. *Auton. Robots* **2013**, *34*, 111–127. [CrossRef]
4. Jetchev, N.; Toussaint, M. Trajectory prediction in cluttered voxel environments. In Proceedings of the 2010 IEEE International Conference on Robotics and Automation (ICRA), Anchorage, AK, USA, 3–7 May 2010; pp. 2523–2528.
5. Yao, Z.; Gupta, K. Path planning with general end-effector constraints. *Robot. Auton. Syst.* **2007**, *55*, 316–327. [CrossRef]
6. Jaillet, L.; Porta, J.M. Path planning under kinematic constraints by rapidly exploring manifolds. *IEEE Trans. Robot.* **2013**, *29*, 105–117. [CrossRef]
7. Berenson, D.; Srinivasa, S.S.; Ferguson, D.; Kuffner, J.J. Manipulation planning on constraint manifolds. In Proceedings of the 2010 IEEE International Conference on Robotics and Automation (ICRA), Kobe, Japan, 12–17 May 2009; pp. 625–632.
8. Suh, C.; Taewoong, T.; Kim, B.; Noh, H.; Kim, M.; Park, F.C. Tangent space RRT: A randomized planning algorithm on constraint manifolds. In Proceedings of the 2010 IEEE International Conference on Robotics and Automation (ICRA), Shanghai, China, 9–13 May 2011; pp. 4968–4973.
9. Berenson, D.; Srinivasa, S.S. Probabilistically complete planning with end-effector pose constraints. In Proceedings of the 2010 IEEE International Conference on Robotics and Automation (ICRA), Anchorage, AK, USA, 3–7 May 2010; pp. 2724–2730.
10. Samson, C.; Borgne, M.L.; Espiau, B. *Robot Control: The Task Function Approach*; Clarendon: Oxford, UK, 1991.
11. Chanand, T.; Dubey, R. A weighted least-norm solution based scheme for avoiding joint limits for redundant joint manipulators. *IEEE Trans. Robot. Autom.* **1995**, *11*, 286–292.
12. Deo, A.S.; Walker, I.D. Minimum effort inverse kinematics for redundant manipulators. *IEEE Trans. Robot. Autom.* **1997**, *13*, 767–775. [CrossRef]
13. Antonelli, G.; Chiaverini, S.; Fusco, G. A new on-line algorithm for inverse kinematics of robot manipulators ensuring path tracking capability under joint limits. *IEEE Trans. Robot. Autom.* **2003**, *19*, 162–167. [CrossRef]
14. Chen, Y.; Li, L.; Ji, X. Smooth and Accurate Trajectory Planning for Industrial Robots. *Adv. Mech. Eng.* **2014**, *6*, 342137. [CrossRef]
15. Zefran, M.; Kumar, V.; Croke, C.B. On the generation of smooth three-dimensional rigid body motions. *IEEE Trans. Robot. Autom.* **1998**, *14*, 576–589. [CrossRef]

16. Chen, Y.; Li, L. Smooth geodesic interpolation for five-axis machine tools. *IEEE/ASME Trans. Mechatron.* **2016**, *21*, 1592–1603. [CrossRef]
17. Rudin, W. *Principles of Mathematical Analysis*, 3rd ed.; McGraw-Hill Companies, Inc.: New York, NY, USA, 1976.